A moving target: responding to magnetic and structural disorder in lanthanide- and actinide-based superconductors

C H Booth[1], E D Bauer[2] and J N Mitchell[3]

[1]Chemical Sciences Division, Lawrence Berkeley National Laboratory, Berkeley, California 94720, USA
[2]Materials Physics and Applications Division, Los Alamos National Laboratory, Los Alamos, New Mexico 87545, USA
[3]Materials Science and Technology Division, Los Alamos National Laboratory, Los Alamos, New Mexico 87545, USA

E-mail: chbooth@lbl.gov

Abstract. The effects of various chemical substitutions and induced lattice disorder in the Ce- and Pu-based 115 superconductors are reviewed, with particular emphasis on results from x-ray absorption fine structure (XAFS) measurements.

1. Introduction

The competition between spin, charge, and lattice interactions is at the heart of many of the strongly-correlated ground states in materials of current interest, such as in colossal magnetoresistors and high-temperature superconductors. This relationship is particularly strong in the CeTIn$_5$ and PuTGa$_5$ series (T = Co, Rh, Ir) of heavy-fermion superconductors. In these systems (figure 1), competition between bulk magnetic and non-magnetic ground states, as well as between superconducting and normal states, are directly related to local properties around the lanthanide or actinide ion, such as the nearest-neighbor bond lengths and the local density of states at the Fermi level. Tiny changes in the latter values can easily tip the balance from one ground state to another. This paper reviews recent work by the authors exploring the relationship between local crystal and electronic structure and ground state magnetic and conducting properties in the Ce- and Pu-based 115 materials.

This work is motivated by the current lack of understanding of superconductivity in the 115 materials, and in heavy-fermion superconductors in general. As if to underscore the complexity in the 115 systems, the superconductivity is not of a conventional type, and may very well not be mediated by a phonon coupling mechanism of the Cooper pairs, but rather by a magnetic coupling mechanism. In the CeRhIn$_5$ system, for instance, superconductivity seems to develop out of the antiferromagnetic state, as shown by the entropy balance at the superconducting transition [1]. Superconductivity in PuCoGa$_5$ is also thought to be magnetically-mediated [2, 3]; however, recent neutron diffraction data cast some doubt on this possibility [4].

The presence of superconductivity in heavy-fermion materials is generally linked with non-Fermi liquid (NFL) behavior and the proximity to a magnetic quantum critical point (QCP).

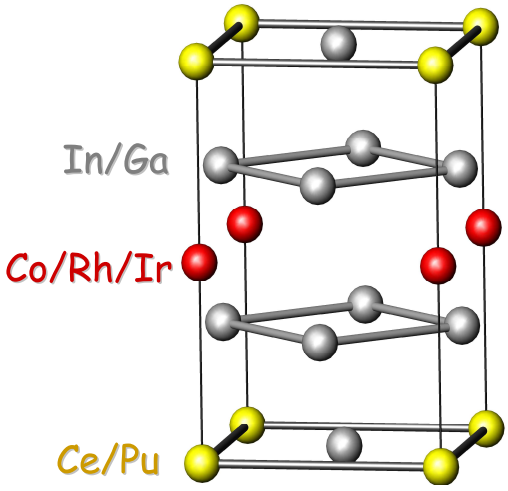

Figure 1. Tetragonal unit cell of the CeTIn$_5$ and PuTGa$_5$ compounds. The In(1) and Ga(1) sites are in the Ce-In and Pu-Ga planes, where as the In(2) and Ga(2) sites flank these planes.

A NFL is a material that does not demonstrate the characteristics of Landau's Fermi liquid theory, whereby conducting properties act like those of a Fermi gas with a renormalized carrier mass. Typical NFL behavior in this class of materials include a non-quadratic temperature dependence of the resistivity in the normal state, and logarithmic or power law divergences in the magnetic susceptibility and the linear electronic coefficient to the heat capacity. NFL behavior is regularly observed around a QCP, and is observed in both CeTIn$_5$ and PuTGa$_5$. In part because of this typical proximity, many researchers believe an associated superconducting state can grow out of quantum fluctuations as one approaches the magnetic phase in the phase diagram. For example, CeRhIn$_5$ is an antiferromagnet in its ground state, but the application of 1.6 GPa precipitates a superconducting phase with strong NFL properties in the normal state [5]. However, the nearby magnetic phase can be obscure. For instance, the observation of an antiferromagnetic phase nearby to CeCoIn$_5$ in its phase diagram was not observed until very recently, when Cd was substituted onto the In sublattice [6]. In PuTGa$_5$, such a phase remains elusive. The so-far observed lack of such a nearby phase has, in fact, prompted an interesting theory that the magnetic and superconducting phases develop simultaneously out of the same normal state, thereby obscuring the magnetic phase [7].

NFL behavior can occur in highly-ordered materials, but is actually more common in materials exhibiting significant amounts of lattice disorder [8]. In these materials, it is possible to model the NFL behavior as due to a distribution of magnetic interaction strengths, either through Kondo interactions alone [9, 10, 11] or through competing Ruderman-Kasuya-Kittel-Yosida (RKKY) and Kondo interactions [12]. One example based on our research is the UCu$_4$Pd system. In that material, the magnetic and heat capacity divergences can be modeled as due to a distribution of Kondo temperatures [9]. Although Pd/Cu site interchange may be at the heart of the required distribution width [11], a model based solely on changes in the f-electron/conduction electron hybridization strength V_{fc} does not quantitatively account for this width [13]. Nevertheless, careful sample annealing can vary the degree of site interchange that exactly tracks the *changes* in divergence of the heat capacity [14], indicating that Kondo disorder at least plays an important role in determining the electronic and magnetic properties of UCu$_4$Pd.

The situation regarding our understanding of the role of local lattice order in the 115 systems therefore revolves around several related issues. Of primary importance is the establishing

of whether the pure 115 materials are as structurally well ordered on the local scale as the diffraction data indicate for the average structure. In addition, since substitutional studies have been invaluable in elucidating details of the ground state, local structure studies need to consider the effect of "foreign" ions on the near-neighbor environment. We employ the extended x-ray absorption fine structure (EXAFS) technique, as it is uniquely able to discern details both regarding local bond order around a majority species through absolute measurements of the mean-squared displacement parameters as a function of temperature, through its sensitivity to these parameters, and because of its ability to gather local structure information even around a dilute species ($\sim 1\%$). This paper reviews such previously published work on the $CeIr_{1-x}Rh_xIn_5$ [15] and $CeT(In_{1-x}M_x)_5$ (M=Sn, Cd, or Hg) [16, 17] series, as well as work reviewing the disordering effects of self-irradiation damage in $PuCoGa_5$ superconductor [18, 19].

2. Establishing a baseline: $CeIr_{1-x}Rh_xIn_5$

The initial local structure studies focused on the $CeIr_{1-x}Rh_xIn_5$ series. $CeRhIn_5$ is an antiferromagnet at ambient pressure that becomes superconducting under applied pressure, peaking at a transition temperature of 2.2 K near 2.1 GPa, and was, in fact, the first of the 115s to demonstrate superconductivity [20]. $CeIrIn_5$ is an ambient pressure superconductor at about 0.4 K. The primary physical interest in the $CeIr_{1-x}Rh_xIn_5$ series is the coexistence of antiferromagnetism and superconductivity from $x \approx 0.4 - 0.7$ [21]; however, from the structural perspective, broad anomalies in the specific heat transitions for intermediate substitution ranges ($0.1 < x < 0.5$) raised the possibility of clustering or other lattice disorder occurring [22]. In addition, it was important to establish the trivalent character of the cerium atom. The aim of the x-ray absorption spectroscopy study was therefore threefold: (1) determine the f-electron count by measuring the Ce $L_{\rm III}$-edge x-ray absorption near-edge structure (XANES); (2) determine the general degree of lattice order or disorder, especially in the end compounds as indicative of the 115 series; and (3) establish the potential amount of Rh or Ir clustering.

XANES spectroscopy is an important tool for measuring the f occupation number, n_f. A heavy-fermion material is related to intermediate valent materials, where V_{fc} is much weaker, but not so weak that the RKKY effect dominates. In this case, the lanthanide or actinide donates a small amount of f-electron density to the conduction band, typically much less than 0.1 electrons per ion. A cerium-based heavy-fermion compound should exhibit a Ce $L_{\rm III}$-edge

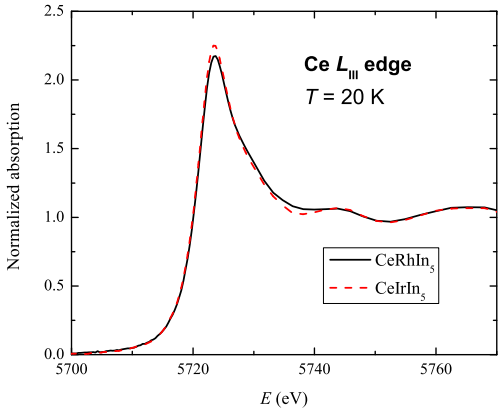

Figure 2. Examples of Ce $L_{\rm III}$-edge XANES at 20 K on $CeRhIn_5$ and $CeIrIn_5$, demonstrating a nearly trivalent state for the cerium atoms.

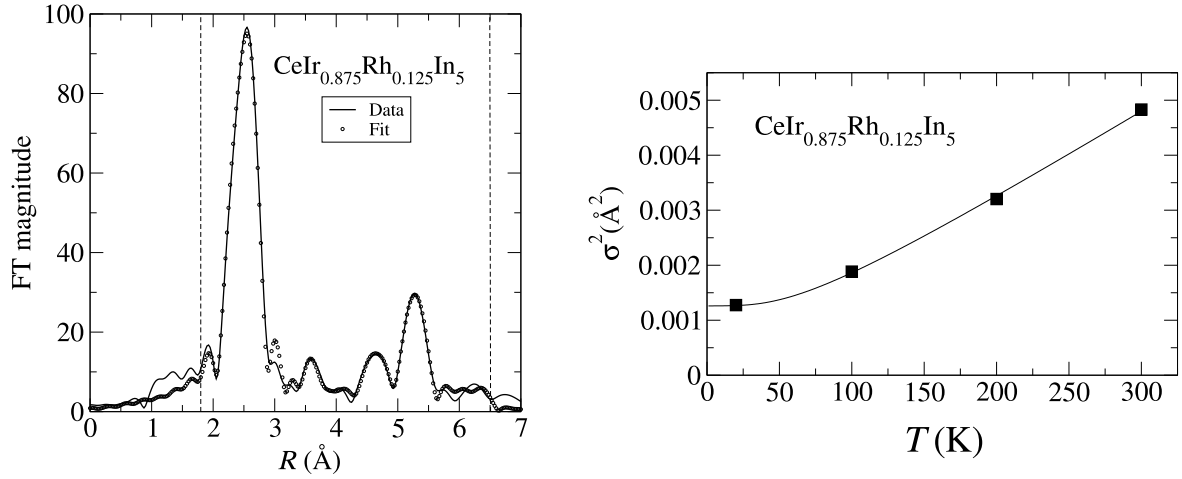

Figure 3. (left) Fourier transform (FT) magnitude of the EXAFS function $k^3\chi(k)$ from Rh K-edge data on $CeIr_{0.875}Rh_{0.125}In_5$, calculated between 3.0 and 15.8 Å^{-1}, with a 0.3 Å^{-1}-wide Gaussian window. (right) Debye-Waller factor for the Ir-In nearest-neighbor scattering pair as a function of temperature. Correlated-Debye model fit indicates $\Theta_{cD} = 259 \pm 6$ K and very little bond disorder, with $\sigma^2_{\rm stat} = -0.0002 \pm 0.0002$ Å^2. This figure is reproduced from reference [15].

spectrum characteristic of trivalent cerium. All of the Ce-115 compounds we have measured display such a spectrum. Figure 2 shows an example for the end compounds at 20 K. Both spectra are dominated by a peak near 5724 eV, characteristic of Ce(III). In addition, a small shoulder is visible near 5730 eV, indicating a small Ce(IV) contribution. As shown in reference [15], this contribution amounts to an n_f of about 0.95±0.03 for all the compounds, and does not change with temperature above 20 K. Differences between the compounds are within the estimated absolute error for the technique, and are probably due, in part, to some oxidation of the samples at their surface.

Determining the degree of local structural order using the EXAFS technique involves several tests. The first requires excellent fits of the model structure to the data, in this case as determined by single-crystal diffraction [23], with reasonable fitted parameter values. Here, it is important to recall that EXAFS is not only a local structural probe like the pair-distribution function (PDF) technique for powder diffraction data [24], but provides PDF data only around the absorbing atomic species, and so provides a partial radial PDF [25]. Consequently, the ideal test using EXAFS of the local bond order is to collect EXAFS data from each atomic species present in the material. Such data were indeed collected in reference [15]; however, In K-edge data were at that time deemed too complicated to gain quantitative information from model fits. Later, during our work on In-site substitutions, we developed a highly constrained fitting model that is, in fact, capable of providing useful information (see section 3). An example of data and a fit to Rh K-edge data with x=0.125 is shown in figure 3. The fitting model includes all single scattering and dominant multiple scattering paths within the fit range, up to 6 Å. As can be seen in the figure, the fit quality is excellent, and is typical of the fits obtained from all edges for these materials. Moreover, the measured pair distances agree well with those expected from the long-range structure [23]. Lastly, the mean-square displacements, otherwise known as the Debye-Waller factors, σ^2, are all small, as expected for a well-ordered intermetallic system.

Another standard test employed is to perform the data collection at several temperatures and track the changes in the measured pair distances and, especially, in σ^2 for selected atom pairs.

The development of σ^2 with temperature is then fit with a correlated-Debye model including an offset, $\sigma^2_{\rm stat}$, that is independent of temperature:

$$\sigma^2 = \sigma^2_{\rm stat} + \sigma^2_{\rm cD}. \quad (1)$$

The correlated-Debye model [26] is similar to the standard Debye model for U^2 parameters in diffraction measurements, except that correlations between the positions of the pairs of atoms, as measured by EXAFS, is taken into account. This model works extremely well for cubic materials [27], but also for more asymmetric systems [28]. In any case, zero-point motions are included, so any non-zero measurement of the offset term $\sigma^2_{\rm stat}$ is indicative of bond length disorder. As can be seen in figure 3, the thermal factors fit the correlated-Debye model well, and in the case displayed, the measured value of $\sigma^2_{\rm stat}$ is consistent with no measurable disorder. Such results are typical for all the measured Ce-based and unaged Pu-based 115 data to date.

3. Preferred-site substitution and "two dimensional" superconductivity: CeT(In$_{1-x}M_x$)$_5$

The studies summarized in section 2 establish the strong degree of crystalline order, both in the end compounds and even as a function of substitution into the transition-metal (T) position in the tetragonal unit cell. Moreover, the effect of such substitutions on the magnetic and electronic properties is relatively weak: one can substitute continuously between Co an Ir, and still obtain a superconductor, and substitutions into CeCoIn$_5$ with Rh don't destroy superconductivity until 60% Rh [29]. Such a weak effect is consistent with the notion that superconductivity is anisotropic in these materials, perhaps even approaching a two-dimensional state. Direct substitution into the Ce layer with La, in fact, has a much more dramatic effect on T_c, destroying superconductivity after only 15% La [30].

Planar substitutions produce even stronger effects when substituting onto the indium site [6, 31, 32, 33, 34, 35], as illustrated in the phase diagram in figure 4. Sn substitution acts more or less like La substitution, except that T_c is reduced much more quickly, going to 0 K after about 3.6% Sn for In. Cd and Hg substitutions are even more dramatic, providing the first access to the sought-after nearby magnetic phase in CeCoIn$_5$ after less than 1% of the indium

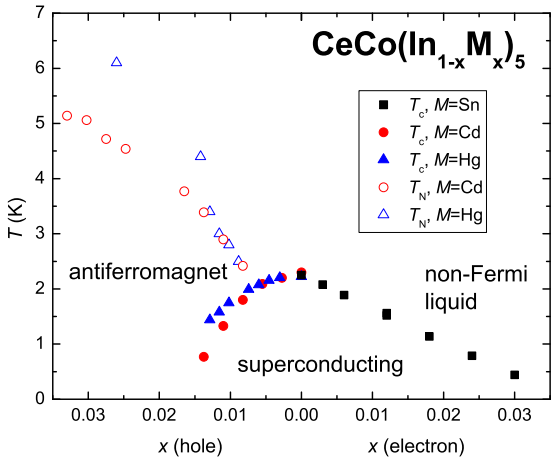

Figure 4. Phase diagram of CeCo(In$_{1-x}M_x$)$_5$ for M=Sn, Cd, and Hg. Relative to indium in the periodic table, Sn acts as an electron dopant and Cd and Hg act as hole dopants. Data are from references [16] and [17].

is replaced. Obviously, not only are the substitutional effects stronger on the indium site than the cerium site, but there are dramatic differences between Sn versus Cd and Hg substitutions. A critical difference between these substituents is the electronic structure: relative to In, Sn has one more electron in the p shell, while Cd and Hg have one less p electron, or rather an electron hole.

Although the electronic structure plays a critical role, the difference in doping dependence between Ce-site and In-site substitutions is strongly dependent on the local substituent distribution within the unit cell. Since Sn, Cd, and Hg substitute onto the In sublattice, there are two positions where the substituents can reside: either into the Ce-In plane on the In(1) site, or flanking it on the In(2) site (figure 1). Moreover, since there is a nearly 0.3 Å difference in the metallic radii between In and the substituents [36], one expects large distortions and, possibly, some ensuing bond length disorder. The EXAFS technique is uniquely poised to answer these questions, since measurements at the Hg L_{III}- and the Sn and Cd K-edges are feasible, even at these low concentrations.

EXAFS data are normalized by the change in absorption at the edge of interest, and are therefore normalized per absorbing atom. From the In K edge, for instance, one obtains a weighted average of the radial PDF from both the In(1) site (20%) and the In(2) site (80%). The key differences in the local environment around each of the two sites is the In(2)-T pair, at about 2.75 Å, and the In(2)-In(2) pair along the c axis, at about 2.9 Å. Other measurable differences exist, including those due to the 4 In-Ce and 8 In-In pairs, all near 3.25 Å, that occur from both In sites. Because of these qualitative differences in the partial radial PDFs, the EXAFS from the substituent edges are very sensitive to the In(1)-site occupancy of the substituent.

Figure 5 shows some typical data from both the Cd and Hg perspectives. The Cd K-edge data display a clear peak near 2.5 Å in the transform, indicative of at least some of the Cd atoms sitting on In(2) sites. (It is vital to note that EXAFS bond lengths are shifted from their position in a Fourier transform, primarily due to phase shifts of the photoelectron at the absorbing and backscattering atoms. These shifts are accurately calculated as a function of the photoelectron wave vector, k, by the FEFF [37] code.) The next major peak at about 3 Å is due to the mixture of In and Ce backscatterers mentioned above. These Cd K-edge data are in stark contrast to the Hg L_{III}-edge data in the lower panel. In those data, no obvious sign of the short Hg(2)-Co and Hg(2)-In(2) peak near 2.5 Å exists. Also, the main In/Ce peak is much larger, and is in fact much closer in magnitude to that observed from the In K edge than the Cd data. From these simple observations we can infer that the Cd environment is distorted, and most of the Hg sits on the the In(1) site.

Because of the phase shifts and other features of the photoelectron backscattering amplitude functions, detailed fits are necessary to extract quantitative information from EXAFS data. In order to allow for so many overlapping peaks and the presence of two possible substituent sites, we developed a fitting model that, at first, constrained several of the bond lengths together [16], and then later developed a more complete model that includes constraints that effectively only allows the lattice constants and the z parameter describing the c axis position of the In(2) planes to vary [17]. With such a model as a starting point, we could release particular constraints to allow for certain distortions to exist. This model allows for fits with many degrees of freedom, and yet still provides excellent fit quality, as seen in figure 5.

The main results of these fits are that, up to the maximum measured concentrations of the substituent (2 to 4% M, depending on the exact system), the fraction of the substituent on the In(1) site, $f_{\mathrm{In}(1)}(M)$, does not vary with concentration. The fraction is, however, a function of the species of M in $\mathrm{CeCo}(\mathrm{In}_{1-x}M_x)_5$, and of T in $\mathrm{Ce}T(\mathrm{In}_{1-x}\mathrm{Hg}_x)_5$. For CeCoIn_5, $f_{\mathrm{In}(1)}(M)$ varies from 43±3%, 55±5%, and 71±5% for M=Sn, Cd, and Hg, respectively. For $\mathrm{Ce}T(\mathrm{In}_{1-x}\mathrm{Hg}_x)_5$, $f_{\mathrm{In}(1)}(M)$ varies from 71±5%, 92±4%, and 100±10% for T=Co, Rh, and Ir, respectively. These

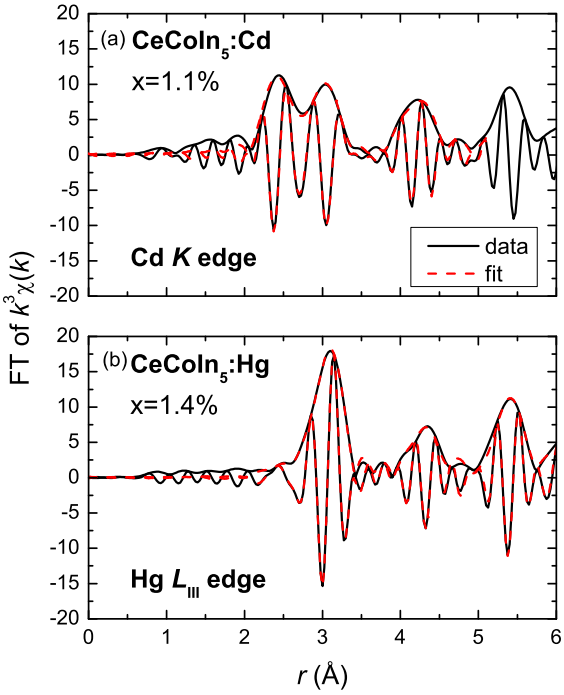

Figure 5. FT of $k^3\chi(k)$ EXAFS data (solid) for typical (a) Cd-substituted and (b) Hg-substituted $CeCoIn_5$ samples. The FT magnitude is indicated by the outer envelope, and the modulating line corresponds to the real part of the transform. Transforms are from 2.5 to 16.0 $Å^{-1}$ and are Gaussian narrowed by 0.3 $Å^{-1}$. This figure is from reference [17].

results exactly track the changes in both the metallic radii of each M and of each T atomic species [36].

These results are of intrinsic interest, since they help explain the strong dependence of T_c on doping concentration and lend credence to the two-dimensional nature of superconductivity in these materials [38], especially when one considers that the mean distance within the planes is similar to the superconducting coherence length in pure $CeCoIn_5$ [39, 40]. These points have been argued [16] in terms of changes in the magnetic impurity concentration, as in an Abrikosov-Gorkov-like mechanism [41]. However, the results from Cd and Hg-substituted samples indicate that site interchange cannot by itself explain the observed trends in the phase diagrams. For instance, although the critical concentration, x_c, where $T_c \to 0$ K decreases with M in the order Sn > Cd > Hg, $f_{\mathrm{In}(1)}(M)$ increases from Cd > Sn > Hg. Even if one ascribes this trend as wholly due to the differences between electron and hole doping, the differences between T_c's in the hole doped materials remains anomalous: until $T_c \to 0$ K, T_c remains higher for all Hg concentrations than for similar Cd concentrations, despite the stronger propensity for Hg to reside on the In(1) site.

In addition to these simple arguments, one can also argue that, since only small differences in V_{fc} are expected for these substituent levels, the major differences in the magnetic and electronic properties must be due to changes in the electronic density of states, possibly due to sharp features in the band structure near the Fermi level as occurs in $YbInCu_4$ [42].

4. Ultimate disorder: radiation damage and superconductivity in $PuCoGa_5$

The previous work on Ce-based 115 materials has been motivated, in part, by the intention to extend the work into the Pu-based 115 materials, especially toward substitutional studies. Unfortunately, due to the myriad of difficulties surrounding working with these samples, there remain very few substitution studies in the Pu 115s at this time [43, 44]. Moreover, the higher radioactivity of most plutonium isotopes, and especially the α decay channel of ^{239}Pu have conspired to create a practically-unique aspect of the Pu-based superconductors: the samples are rapidly destroying themselves. Even in the first paper on $PuCoGa_5$, Sarrao *et al.* [45] noted that T_c fell by about 0.25 K per month. Also in that original work it was noted that many of the interesting properties of $PuCoGa_5$ are likely related to self-irradiation damage from the α-decay of the Pu nucleus, such as the very high critical current density and upper critical field. Subsequent studies by the Wastin group [46, 47, 48] have focused on this self-irradiation damage as a way to probe the superconducting state, tracking changes in various properties such as the electrical resistivity until the materials are finally no longer superconducting [48]. Changes in other properties have also been observed with time, such as in the superfluid density as probed by muon spin relaxation measurements [49].

Although recent advances in Molecular Dynamics calculations have lead to a much better understanding of radiation damage effect over the last 15 years [50], state-of-the-art calculations including plutonium atoms in intermetallic materials have only recently become possible [51] and have yet to be performed for $PuCoGa_5$. It is possible, however, to infer upper limits of the material fraction that undergoes radiation damage by comparing with the case of Pu-Ga alloys. The main damage from the α-decay of a Pu atom is due to permanent displacements of nearby atoms in the lattice by ballistic interaction with the 86 keV ^{235}U recoil nucleus (see reference [52] for a good overview), producing a damage cascade over several nanometers. The number of interstitial/vacancy defect pairs produced in each decay in elemental Pu is estimated to be about $N_D \approx 2500$ Frenkel defect pairs, and the situation is expected to be similar for $PuCoGa_5$ [53]. The samples discussed below have an α-decay rate of $\lambda_\alpha \approx 3.4 \times 10^{-5}\alpha$-decays per Pu atom per year. The fraction of defect sites in $PuCoGa_5$ is therefore estimated to be $f_D = 2N_D\lambda_\alpha/7 \approx 2.5\%$ per year, since a Frenkel defect includes both the interstitial and the vacancy and 1/7 of the atoms are Pu. This estimate does not account for the relaxation of the lattice around each defect, which can reduce the number of defects by between 50 and 90% [54], nor does it account for any lattice distortions around a defect. The latter quantity is typically ignored in discussion and calculations of radiation damage, but is likely important for explaining discrepancies between such calculations and actual damage estimates using probes sensitive to the local structure, such as nuclear magnetic resonance experiments [55, 56].

The EXAFS technique is sensitive to both defects and distortions. Since the photoelectron backscattering probability for a shell of atoms at a given distance around the absorption goes approximately as $1/\sigma$, atoms in highly distorted sites like interstitials will make virtually no contribution to the EXAFS signal. A damage fraction estimate based on the scattering amplitude of the first Pu-Ga scattering shell will thus provide a lower limit to the total fraction of displaced atoms. This model has also been extended to include more moderate lattice relaxation that generates a small enough σ to provide a detectable signal [19]. The total estimated fraction of atoms that have been displaced, including the roughly 5% that are moderately displaced, is shown in figure 6 as previously published [19] for two $PuCoGa_5$ samples, in addition to preliminary data on a sample of $PuAl_2$ and two samples of $PuGa_3$ [43]. The "maximum range" shown is the estimate of the damaged fraction only from the defect production, not including any lattice relaxation. It is important to note that the abscissa is in units of α-decays per atom in the formula unit; that is, $\lambda_\alpha/7$ for $PuCoGa_5$, $\lambda_\alpha/4$ for $PuGa_3$ and $\lambda_\alpha/3$ for $PuAl_2$. One year corresponds to about $5 \times 10^{-6}\alpha$-decays per atom for $PuCoGa_5$.

There are a number of interesting features of these results. The first is that the damage

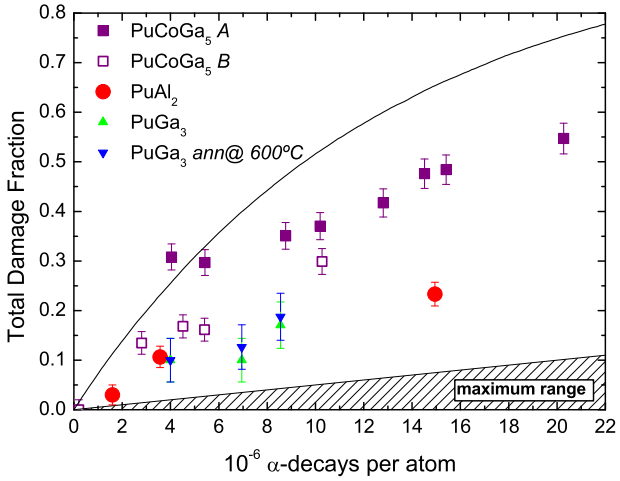

Figure 6. Total damage fraction as determined from the Pu L_{III}-edge EXAFS for two samples of $PuCoGa_5$, two of $PuGa_3$, and a sample of $PuAl_2$, using methods outlined in references [18] and [19]. The region marked "maximum range" is the damage assuming full Frenkel-pair defect production with no further lattice relaxation, as well as no further lattice response beyond the placement of the interstitial and vacancy defects. The solid line represents a percolation model with a time scale chosen to agree with the early ($< 5 \times 10^{-6}\alpha$-decays per atom) data from $PuCoGa_5$ Sample A.

accumulates at a rate much faster than expected including defect production alone for all the samples. We therefore conclude that lattice distortions are not only important, but dominate the contribution to the total damage fraction. In order to achieve such a high damage accumulation rate, lattice distortions would have to occur at least partially in the second coordination shell around the defect. Given a cascade volume of order 500 nm^3, second coordination shell distortions would indicate that virtually every atom within a damage cascade is distorted significantly from its original lattice position. Such damage then becomes qualitatively similar to Seitz's "thermal spike" model [57], whereby the recoil nucleus causes a local melting and fast quench of the entire cascade region.

Most of the damage occurs within the first year, and then appears to slow down, especially in the $PuCoGa_5$ samples. Such a slowing down is expected in a percolation model, since as cascade regions begin to overlap, the damage fraction will no longer increase linearly. Such a model is shown in figure 6, with the time scale chosen to agree with data from Sample A within the first year. However, extrapolating the data with relatively few total decays with a percolation model does not reproduce the data with more decays. Since the samples are all stored at room temperature, these data emphasize the role of annealing at room temperature in plutonium intermetallics. This result is not unexpected, since δ-Pu is now well known to undergo significant annealing, even at temperatures as low as 30 K [58]. In fact, the T_c of a $PuCoGa_5$ sample stored at temperatures below 30 K has been shown from Meissner effect measurements to decrease nearly twice as fast ($\approx$ 0.5 K/mo [59]) compared to those stored at room temperature (0.25 K/mo [19, 45]) Clearly, these samples undergo significant annealing at or below room temperature. In fact, if one considers only the damage cascade production, the percolation line in figure 6 indicates the percolation limit (around 20% in three dimensions) will be reached near $25 \times 10^{-6}\alpha$-decays per atom, or in about 5 years. This value is consistent with recent data by Jutier and co-workers [48] that indicates superconductivity in $PuCoGa_5$ is

destroyed after somewhat more than 4 years in similar samples. Such a model assumes that even though some damage gets annealed away in a given cascade over time, sufficient damage exists to prevent the cascade region from superconducting. It is also possible to understand these data and the reduction of T_c in terms of strong scattering in a short coherence length superconductor [19].

Data from the non-$PuCoGa_5$ samples, while preliminary, are also interesting, especially in contrast to the $PuCoGa_5$ data. Of the five samples measured, the oldest sample is $PuCoGa_5$ Sample A, and it appears to show the largest damage accumulation rate. The $PuGa_3$ and $PuAl_2$ samples are fairly similar to $PuCoGa_5$ Sample B. We do not know of any reason Sample A should be different from Sample B, as they were both stored in the same cabinet in the same laboratory, although Sample A is, indeed, about two years older. Clearly, to gain the best understanding of radiation damage effects, one should store the samples in a better-controlled environment. Also, it is well known that the melting temperature correlates with the propensity for damage, with a higher melting point corresponding to fewer defects produced per α-decay [60]. The melting points of these compounds are not presently known, but, other than $PuCoGa_5$ Sample A, they have remarkably similar damage production rates. It is also interesting to note that the annealed $PuGa_3$ sample is plotted as a function of the decays since synthesis, which was several months before it was annealed; one needs to subtract about $4 \times 10^{-6}\alpha$-decays per atom to obtain the number of decays since it was annealed. These data indicate that, at least with regards to the local structure, annealing $PuGa_3$ at 600°C is virtually equivalent to annealing at room temperature. Clearly, more systematic studies including melting point determination and annealing properties are warranted.

Although not shown in figure 6, the EXAFS data have also been analyzed from the Co and Ga K edges [19], and it appears that the local structure around those absorbing atoms shows smaller distortions than around the Pu atoms. A probable explanation is that the lighter atoms are more likely than the heavy Pu atoms to be ejected from their equilibrium lattice positions to the outer edges of a cascade region. A similar inhomogeneity has, in fact, been featured in Molecular Dynamics calculations of uranium recoils in zircon [61].

As a final note, these results underscore much of what remains unknown regarding both superconductivity and radiation damage effects in $PuCoGa_5$. Although the surprisingly large amount of damage observed explains the bulk of the reduction of T_c with time, many of the exact details have not been addressed. For instance, one might expect the reduction of T_c *not* to be linear with time, and rather to be proportional to the damage fraction in figure 6. In contrast, most of the damage occurs within the first year, and annealing is known to affect the local distortions. Another aspect that has not been thoroughly explored is the presence of non-Fermi liquid behavior, which is expected to become more dominant as the sample is further disordered [9, 10, 11]. Together with measurements of the local distortions, one should be able to compare the distortions with the development of logarithmic divergences in the magnetic susceptibility, for instance. Perhaps even more importantly, under appropriate experimental conditions, one should be able to directly compare local structure measures of damage with the results of modern Molecular Dynamics simulations, and thus provide some of the first atomic-scale verifications of the theories of both lattice relaxation and Frenkel defect production.

5. Conclusions

The $PuCoGa_5$ system offers the opportunity to follow changes in magnetic and electronic properties due to lattice disorder as a function of time in the same samples, in addition to the more traditional approach of perturbing the superconducting state through chemical substitutions. The reviewed work establishes a baseline for such future studies by determining the intrinsic lattice order in the 115 system, successfully understanding disorder as introduced through chemical substitutions in the Ce-based 115s, and beginning to explore the surprisingly

large role of self-irradiation damage directly on the $PuCoGa_5$ lattice. These studies lay the foundation for the harder future work toward measuring chemical substitutions in $PuCoGa_5$, correlating effects with non-Fermi liquid behavior, and obtaining a better structural picture of the distortions induced by α-decay of the plutonium nucleus.

Acknowledgments
Work at Lawrence Berkeley National Laboratory was supported by the Director, Office of Science, Office of Basic Energy Sciences, of the U.S. Department of Energy (DOE) under Contract No. DE-AC02-05CH11231. X-ray data were collected at the Stanford Synchrotron Radiation Lightsource, a national user facility operated by Stanford University on behalf of the DOE, Office of Basic Energy Sciences. Work at Los Alamos was supported under the auspices of the DOE.

References

[1] Park T and Thompson J D 2009 *New J. Phys.* **11** 055062
[2] Bauer E D, Thompson J D, Sarrao J L, Morales L A, Wastin F, Rebizant J, Griveau J C, Javorsky P, Boulet P, Colineau E, Lander G H and Stewart G R 2004 *Phys. Rev. Lett.* **93** 147005
[3] Curro N J, Caldwell T, Bauer E D, Morales L A, Graf M J, Bang Y, Balatsky A V, Thompson J D and Sarrao J L 2005 *Nature (London)* **434** 622
[4] Hiess A, Stunault A, Colineau E, Rebizant J, Wastin F, Caciuffo R and Lander G H 2008 *Phys. Rev. Lett.* **100** 076403
[5] Park T, Ronning F, Yuan H Q, Salamon M B, Movshovich R, Sarrao J L and Thompson J D 2006 *Nature (London)* **440** 65
[6] Pham L D, Park T, Maquilon S, Thompson J D and Fisk Z 2006 *Phys. Rev. Lett.* **97** 056404
[7] Flint R, Dzero M and Coleman P 2008 *Nat. Phys.* **4** 643
[8] Stewart G R 2001 *Rev. Mod. Phys.* **73** 797
[9] Bernal O O, MacLaughlin D E, Lukefahr H G and Andraka B 1995 *Phys. Rev. Lett.* **75** 2023
[10] Miranda E, Dobrosavljević V and Kotliar G 1997 *Phys. Rev. Lett.* **78** 290
[11] Booth C H, MacLaughlin D E, Heffner R H, Chau R, Maple M B and Kwei G H 1998 *Phys. Rev. Lett.* **81** 3960
[12] Castro Neto A H, Castilla G and Jones B A 1998 *Phys. Rev. Lett.* **81** 3531
[13] Bauer E D, Booth C H, Kwei G H, Chau R and Maple M B 2001 *Phys. Rev.* B **65** 245114
[14] Booth C H, Scheildt E W, Killer U, Weber A and Kehrein S 2002 *Phys. Rev. B* **66** 140402(R)
[15] Daniel M, S-W Han, Booth C H, Cornelius A L, Pagliuso P G, Sarrao J L and Thompson J D 2005 *Phys. Rev.* B **71** 054417
[16] Daniel M, Bauer E D, S-W Han, Booth C H, Cornelius A L, Pagliuso P G and Sarrao J L 2005 *Phys. Rev. Lett.* **95** 016406
[17] Booth C H, Bauer E D, Bianchi A D, Ronning F, Thompson J D, Sarrao J L, Cho J Y, Chan J Y, Capan C and Fisk Z 2009 *Phys. Rev.* B **79** 144519
[18] Booth C H, Daniel M, Wilson R E, Bauer E D, Mitchell J N, Moreno N O, Morales L A, Sarrao J L and Allen P G 2007 *J. Alloys and Compds.* **444** 119
[19] Booth C H, Bauer E D, Daniel M, Wilson R E, Mitchell J N, Morales L A, Sarrao J L and Allen P G 2007 *Phys. Rev.* B **76** 064530
[20] Hegger H, Petrovic C, Moshopoulou E G, Hundley M F, Sarrao J L, Fisk Z and Thompson J D 2000 *Phys. Rev. Lett.* **84** 4986
[21] Pagliuso P G, Petrovic C, Movshovich R, Hall D, Hundley M F, Sarrao J L, Thompson J D and Fisk Z 2001 *Phys. Rev. B* **64** 100503(R)
[22] Bianchi A, Movshovich R, Jaime M, Thompson J D, Pagliuso P G and Sarrao J L 2001 *Phys. Rev. B* **64** 220504
[23] Moshopoulou E G, Fisk Z, Sarrao J L and Thompson J D 2001 *J. Solid State Chem.* **158** 25
[24] Egami T and S J L Billinge 2003 *Underneath the Bragg peaks: Structural analysis of complex materials* (Amsterdam: Pergamon)
[25] Teo B K 1986 *EXAFS: Basic Principles and Data Analysis* (New York: Springer-Verlag)
[26] Crozier E D, Rehr J J and Ingalls R 1988 *X-Ray Absorption: Principles, Applications, Techniques of EXAFS, SEXAFS, XANES* ed Konigsberger D and Prins R (New York: Wiley) p 373
[27] Li G G, Bridges F and Booth C H 1995 *Phys. Rev.* B **52** 6332

[28] Booth C H, Bridges F, Kwei G H, Lawrence J M, Cornelius A L and Neumeier J J 1998 *Phys. Rev. B* **57** 10440
[29] Zapf V S, Freeman E J, Bauer E D, Petricka J, Sirvent C, Frederick N A, Dickey R P and Maple M B 2001 *Phys. Rev. B* **65** 014506
[30] Petrovic C, Bud'ko S L, Kogan V G and Canfield P C 2002 *Phys. Rev. B* **66** 054534
[31] Bauer E D, Moreno N O, Mixson D J, Sarrao J L, Thompson J D, Hundley M F, Movshovich R and Pagliuso P G 2005 *Physica B* **359** 35
[32] Bauer E D, Capan C, Ronning F, Movshovich R, Thompson J D and Sarrao J L 2005 *Phys. Rev. Lett.* **94** 047001
[33] Bauer E D, Mixson D, Ronning F, Hur N, Movshovich R, Thompson J D, Sarrao J L, Hundley M F, Tobash P H and Bobev S 2006 *Physica B* **378-380** 142
[34] Bauer E D, Ronning F, Capan C, Graf M J, Vandervelde D, Yuan H Q, Salamon M B, Mixson D J, Moreno N O, Brown S R, Thompson J D, Movshovich R, Hundley M F, Sarrao J L, Pagliuso P G and Kauzlarich S M 2006 *Phys. Rev. B* **73** 245109
[35] Nicklas M, Stockert O, Park T, Habicht K, Kiefer K, Pham L D, Thompson J D, Fisk Z and Steglich F 2007 *Phys. Rev. B* **76** 052401
[36] Clementi E, Raimondi D L and Reinhardt W P 1967 *J. Chem. Phys.* **47** 1300
[37] Ankudinov A L and Rehr J J 1997 *Phys. Rev.* B **56** R1712
[38] Monthoux P and Lonzarich G G 2001 *Phys. Rev. B* **63** 054529
[39] Settai R, Shishido H, Ikeda S, Murakawa Y, Nakashima M, Aoki D, Harima Y H H and Onuki Y 2001 *J. Phys. Condens. Matter* **13** L627
[40] M-R Eskildsen, Dewhurst C D, Hoogenboom B W, Petrovic C and Canfield P C 2003 *Phys. Rev. Lett.* **90** 187001
[41] Abrikosov A A and Gor'kov L P 1961 *Sov. Phys. JETP* **12** 1243
[42] Antonov V N, Galli M, Marabelli F, Yaresko A N, Perlov A Y and Bauer E 2000 *Phys. Rev. B* **62** 1742
[43] Boulet P, Colineau E, Wastin F, Rebizant J, Javorský P, Lander G H and Thompson J D 2005 *Phys. Rev.* B **72** 104508
[44] Javorský P, Jutier F, Boulet P, Wastin F, Colineau E and Rebizant J 2006 *Physica* B **378-380** 1007
[45] Sarrao J L, Morales L A, Thompson J D, Scott B L, Stewart G R, Wastin F, Rebizant J, Boulet P, Colineau E and Lander G H 2002 *Nature (London)* **420** 297
[46] Jutier F, Griveau J C, Colineau E, Rebizant J, Boulet P, Wastin F and Simoni E 2005 *Physica B* **359-361** 1078
[47] Jutier F, Griveau J C, Van Der Beek C J, Colineau E, Wastin F, Rebizant J, Boulet P, Wiss T, Thiele H and Simoni E 2007 *EPL* **78** 57008
[48] Jutier F, Ummarino G A, Griveau J C, Wastin F, Colineau E, Rebizant J, Magnani N and Caciuffo R 2008 *Phys. Rev.* B **77** 024521
[49] Ohishi K, Heffner R H, Morris G D, Bauer E D, Graf M J, Zhu J X, Morales L A, Sarrao J L, Fluss M J, MacLaughlin D E, Shu L, Higemoto W and Ito T U 2007 *Phys. Rev.* B **76** 064504
[50] Averback R S and Diaz de la Rubia T 1998 *Solid State Physics* vol 51 ed Ehrenreich H and Spaepen F (New York: Academic) p 281
[51] Kubota A, Wolfer W G, Valone S M and Baskes M I 2007 *J. Comput.-Aid. Mater. Des.* **14** 367
[52] Wolfer W G 2000 *Los Alamos Sci.* **26** 274 and references therein
[53] http://www.srim.org/
[54] Diaz de la Rubia T, Caturla M J, Alonso E A, Soneda N and Johnson M D 1999 *Radiation Effects and Defects in Solids* **148** 95–126
[55] Farnan I and Salje E K H 2001 *J. Appl. Phys.* **89** 2084
[56] Farnan I, Cho H and Weber W J 2007 *Nature (London)* **445** 190
[57] Seitz F 1949 *Disc. Faraday Soc.* **5** 271
[58] Fluss M J, Wirth B D, Wall M, Felter T E, Caturla M J, Kubota A and Diaz de la Rubia T 2004 *J. Alloys Compd.* **368** 62
[59] McCall S K private communication
[60] Kinchin G H and Pease R S 1955 *Rep. Prog. Phys.* **18** 1
[61] Devanathan R, Corrales L R, Weber W J, Chartier A and Meis C 2006 *Mol. Simul.* **32** 1069